Comparison of implicit-texture and population-balance foam models

Lotfollahi, M; Farajzadeh, R; Delshad, M; Varavei, A; Rossen, WR

DOI
10.1016/j.jngse.2016.03.018

Publication date
2016

Document Version
Final published version

Published in
Journal of Natural Gas Science and Engineering

Journal of Natural Gas Science and Engineering 31 (2016) 184–197

Contents lists available at ScienceDirect

Journal of Natural Gas Science and Engineering

journal homepage: www.elsevier.com/locate/jngse

Comparison of implicit-texture and population-balance foam models

Mohammad Lotfollahi [a], Rouhi Farajzadeh [b, c, *], Mojdeh Delshad [a], Abdoljalil Varavei [a], William R. Rossen [b]

[a] University of Texas at Austin, USA
[b] Delft University of Technology, The Netherlands
[c] Shell Global Solutions International, Rijswijk, The Netherlands

ARTICLE INFO

Article history:
Received 16 November 2015
Received in revised form
3 March 2016
Accepted 4 March 2016
Available online 9 March 2016

Keywords:
Foam
Implicit texture
Population balance
Modeling
Gas
Enhanced oil and gas recovery

ABSTRACT

Simulation models for foam enhanced oil recovery are of two types: those that treat foam texture or bubble size explicitly (population-balance models) and those that treat the effects of foam texture implicitly through a gas mobility-reduction factor. The implicit-texture models all implicitly assume local equilibrium (LE) between the processes of foam creation and destruction. In published studies most population-balance models predict rapid attainment of local-equilibrium as well, and some have been recast in LE versions.

In this paper we compare population-balance and implicit-texture (IT) models in two ways. First, we show the equivalence of the two approaches by deriving explicitly the foam texture and foam-coalescence-rate function implicit in the IT models, and then show its similarity to that in population-balance models. Second, we compare the models based on their ability to represent a set of N_2 and CO_2 steady-state foam experiments and discuss the corresponding parameters of the different methods.

Each of the IT models examined was equivalent to the LE formulation of a population-balance model with a lamella-destruction function that increases abruptly in the vicinity of the limiting capillary pressure P_c^*, as in current population-balance models. The relation between steady-state foam texture and water saturation or capillary pressure implicit in the IT models is essentially the same as that in the population-balance models. The IT and population-balance models match the experimental data presented equally well. The IT models examined allow for flexibility in making the abruptness of the coalescence rate near P_c^* an adjustable parameter. Some allow for coarse foam to survive at high capillary pressure, and allow for a range of power-law non-Newtonian behavior in the low-quality regime.

Thus the IT models that incorporate an abrupt change in foam properties near a given water saturation can be recast as LE versions of corresponding population-balance models with a lamella-destruction function similar to those in current PB models. The trends in dimensionless foam texture implicit in the IT models is similar to that in the PB models. In other words, both types of model, at least in the LE approximation, equally honor the physics of foam behavior in porous media.

1. Introduction

Enhanced oil recovery (EOR) techniques such as solvent, thermal, and chemical injection have the potential to increase oil production and oil recovery efficiency (Lake et al., 2014). With growth of global energy demand there is a significant interest by the oil industry in the development, optimization, and implementation of EOR methods.

Mobility control is essential to the effectiveness of EOR processes, such as surfactant/alkali flooding, miscible and immiscible gas flooding, and steam flooding. Gas-injection EOR projects often suffer from poor volumetric sweep efficiency due to low gas density and viscosity. The use of foam in gas-injection EOR applications has the potential to improve oil recovery by reducing gas mobility (Schramm, 1994; Kovscek and Radke, 1994; Rossen, 1996; Farajzadeh et al., 2011; Andrianov et al. 2012).

Foam in porous media can be defined as a dispersion of gas phase in liquid phase such that the liquid phase is connected and at least some gas flow paths are blocked by thin liquid films, called lamellae (Falls et al., 1988). It has been experimentally observed

* Corresponding author. Delft University of Technology, The Netherlands.
E-mail address: R.Farajzadeh@tudelft.nl (R. Farajzadeh).

http://dx.doi.org/10.1016/j.jngse.2016.03.018

that when gas/water capillary pressure in a porous medium approaches a certain value, the foam coarsens abruptly; this value referred to as the "limiting capillary pressure", and the corresponding saturation is called "limiting water saturation", S_w^* (Khatib et al., 1988; Zhou and Rossen, 1995). The limiting capillary pressure is a function of surfactant formulation and concentration, electrolyte concentration, formation properties such as permeability, and other factors (Khatib et al., 1988; Farajzadeh et al., 2015). The limiting-capillary-pressure concept is illustrated in Fig. 1.

In the absence of oil, foam exhibits two steady-state flow regimes (Osterloh and Jante, 1992; Alvarez et al., 2001; Chen et al., 2010). In the "low quality" (i.e., low gas fractional flow) or "wet" regime, the foam bubble size remains near the average pore size and pressure gradient is nearly independent of liquid velocity. In the "high-quality", "dry-out" or "coalescence" regime, bubble size increases and foam becomes coarser over a narrow range of water saturation. In the high-quality regime, pressure gradient is nearly independent of gas superficial velocity.

The limiting capillary pressure is thought to regulate foam behavior in the high-quality regime as follows. Suppose foam is at local equilibrium in the high-quality regime. The capillary pressure just below P_c^*. Then suppose gas velocity increases by a factor X at constant water superficial velocity. As a result, water saturation falls slightly. Capillary pressure P_c approaches a bit closer to P_c^*. The approach to P_c^* causes a large increase in coalescence rate (Ettinger and Radke, 1992; Aronson and Radke, 1994), coarsening the foam and raising gas mobility by the same factor X with little or no change in water saturation. The decrease in water saturation is slight, so water saturation and water relative permeability are nearly unchanged. Therefore, LE is restored with the same pressure gradient as before the increase in gas superficial velocity. Foam is near P_c^* in the high-quality or coalescence regime and the abrupt increase in coalescence rate as P_c approaches P_c^* is responsible for foam behavior in this regime.

Design of foam EOR processes for field application requires accurate simulation models. Foam simulation models come in two types: Population-balance (PB) models attempt to represent the dynamic processes of lamella creation and destruction as well as the effect of bubble size on gas mobility. These models can be set to assume local equilibrium (LE) between the processes of lamella creation and destruction. The second group of models reflects the effects of foam texture implicitly through a gas mobility-reduction factor that depends on saturations, superficial velocities and other factors. These models all assume LE. To avoid confusion with the LE version of PB models we refer to the second group here as implicit-texture (IT) models. PB models are often assumed to be better because they are based on first principles. The dynamic version of the models are sometimes called "full physics" models (Chen et al., 2010; Ma et al., 2015). The IT models are often referred to as "empirical" (Rossen et al., 1999) or "semi-empirical" and lacking in essential physics (Kovscek et al., 1995; Chen et al., 2010; Skoreyko et al., 2012; Ma et al., 2015). Ma et al. (2015) review a wide range of foam models and their assumptions. All models, of course, incorporate only partial and imperfect physics. An essential test for models is their ability to fit available data.

Skoreyko et al. (2012) represent foam generation, foam degradation and trapped foam by defining a set of first order, non-reversible reactions. They use Arrhenius-type equations to compute reaction rates. This model makes no reference to foam coarsening at a limiting capillary pressure, however, which distinguishes it from the models described here. Likewise, the population-balance models of Falls et al. (1988), Friedmann et al. (1991) and Zitha (2006) do not include foam coalescence at a limiting capillary pressure. Therefore, we do not address these models further in this paper.

In all the foam models discussed here, foam coalescence is related to P_c^*. In the PB models, P_c^*, or its corresponding saturation, S_w^*, is explicitly specified as an input parameter to calculate the coalescence rate and bubble size. The IT models incorporate P_c^* implicitly by employing the limiting water saturation S_w^* as an input parameter. In PB models foam collapses as capillary pressure approaches P_c^* or S_w approaches S_w^*, while in the IT models foam collapse occurs when foam becomes too dry i.e. in the vicinity of S_w^*. The IT models differ from each other in whether foam collapses completely, or degrades partially, in the vicinity of S_w^* (Cheng et al., 2000).

This paper investigates the limiting-capillary-pressure concept as applied in both IT and PB models. Specifically, it shows that the limiting water saturation in IT models can be expressed as a coalescence (destruction) term in an equivalent way to that in PB models. Moreover, the foam texture implicit in these models can be derived; it abruptly coarsens near P_c^* as in the PB models. In other words, each IT model examined is equivalent to the LE formulation of a corresponding population-balance model: the physics of foam

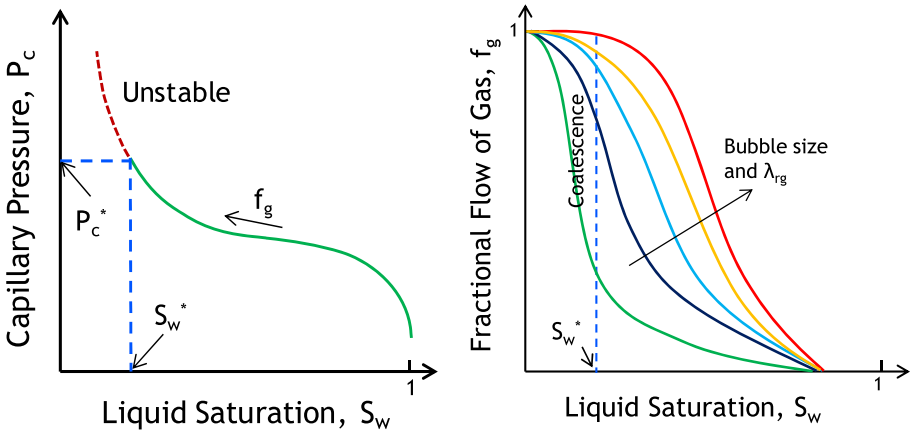

Fig. 1. Limiting-capillary-pressure (P_c^*) concept (adapted from Khatib et al., 1988). The right-hand figures shows the fractional-flow curves for different fixed bubbles sizes, but P_c and S_w control bubble size at LE. For $P_c < P_c^*$ ($S_w > S_w^*$) bubble size is small and the green fractional-flow curve applies. Approaching the limiting capillary pressure from lower P_c (approaching S_w^* from higher S_w) bubble size increases, gas mobility rises and gas fractional flow in the porous medium increases. If the transition is abrupt, the "high-quality" foam regime is at $S_w = S_w^*$ (dotted line), and the low-quality regime is at $S_w > S_w^*$ (on the green curve). (For interpretation of the references to colour in this figure legend, the reader is referred to the web version of this article.)

coalescence as represented in the two types of models is essentially the same, at least under the conditions of the given experiments.

In addition, the experimental data for steady-state apparent foam viscosity (without oil present) versus foam quality are matched with the different foam models and the corresponding parameters in each model are discussed. The results confirm that the steady-state flow of foam in porous media can be adequately represented equally well by the simpler IT models.

Only population-balance models can represent the dynamics of foam creation and propagation at a shock front, the creation of foam at the entrance of the porous medium or near an abrupt change in permeability, and, possibly, foam dynamics in natural fractures. However, in published applications, PB models come to local equilibrium rapidly, suggesting that on the field scale LE applies, at least in relatively homogeneous formations (Rossen et al., 1999; Chen et al., 2010). The first step in fitting any foam model is to examine its ability to represent laboratory LE data, and this study focuses on that issue.

2. Foam models

Nearly all foam models alter the transport properties of gas only and assume that liquid mobility remains the same function of saturations as in the absence of foam, in accordance with laboratory observations (Bernard and Holm, 1964; Bernard et al., 1965; Sanchez et al., 1989; de Vries and Wit, 1990; Friedmann et al., 1991). In the presence of foam, gas trapped by stationary lamellae reduces mobile gas saturation, blocks gas flow and alters gas flow paths, and thus reduces gas relative permeability. The fraction of trapped gas is a function of pressure gradient, capillary pressure, aqueous-phase saturation, pore geometry and bubble size (Kovscek et al., 1995; Nguyen et al., 2007, 2009). On the other hand, moving lamellae experience a drag force when they slide along the pore walls (Hirasaki and Lawson, 1985) that is complicated by capillary effects on the lamellae (Falls et al., 1989; Xu and Rossen, 2003). This effect is similar to an increase in gas viscosity. Because the viscosity of gas itself is not increased by foam, the effect of increased resistance to gas flow reflecting the presence of lamellae is termed "apparent (effective) gas viscosity." However, many models combine the effects of foam on gas relative permeability and apparent gas viscosity and reduce the gas mobility by a factor applied to either the gas viscosity or the gas relative permeability. In the following sections, IT and PB foam models are briefly discussed. Appendix A and Ma et al. (2015) provide a review of foam models.

2.1. Implicit-texture (IT) models

In this section we briefly discuss the UT (Cheng et al. (2000)), STARS (Computer Modeling Group, 2012) and Vassenden-Holt (1998) IT models. A summary of these models is provided in Table (A-1).

2.1.1. UT model

The UT model (Rossen et al., 1999; Cheng et al., 2000) was originally based on data of Persoff et al. (1991), which lies entirely in the high-quality regime. At fixed gas superficial velocity, this model gives a steep, linear increase in gas mobility as water saturation decreases through a narrow interval in the immediate vicinity of S_w^*, and a constant reduction in gas mobility for larger values of S_w. The model allows for non-Newtonian behavior in the low-quality regime by making the mobility-reduction factor in the low-quality regime a power-law function of gas superficial velocity. This model is currently in use in compositional simulator UTDOECO2 (Delshad et al., 2013; Naderi Beni et al., 2013) and chemical-flood simulator UTCHEM (Delshad, 2013). Because of the functional form chosen for the increase in gas mobility near S_w^*, the UT foam model cannot represent formation of strong foam during gas injection in a process of injection of alternating slugs of gas and surfactant solution (Dong, 2001; Shan and Rossen, 2004).

2.1.2. STARS model

In the STARS model (Computer Modeling Group (CMG), 2012), when foam is present, the gas relative permeability is multiplied by a factor *FM*, which is function of several factors that reflect the effects of different physical parameters, such as surfactant concentration, water saturation, oil saturation (and composition), salt concentration, and capillary number on foam behavior in porous media. In this paper, we focus on the dry-out function F_2 and shear-thinning function F_5, which are defined in Table (A-1). As in the UT model, gas mobility increases as S_w decreases in the vicinity of S_w^*, which is given the name *fmdry* in the STARS model. However, in the STARS model foam does not collapse completely at any water saturation. The function F_5 allows for shear-thinning in the low-quality regime by making the mobility-reduction factor depend on capillary number (i.e., on pressure gradient).

2.1.3. Vassenden-Holt model

Vassenden and Holt (1998) proposed a foam simulation model in which the gas mobility reduction factor, *F*, is the sum of two exponential functions of water saturation. For water saturation slightly greater than S_f (equivalent to S_w^*), gas mobility decreases steeply because of the first exponential function; this corresponds to foam dryout and the high-quality regime. The second function decreases more gradually for higher water saturation and controls foam behavior in the low-quality regime.

2.2. Population-balance (PB) models

Foam mobility is influenced by its texture (Patzek, 1988; Falls et al., 1988). Foam texture is quantified as the number of lamellae per unit volume of gas. A foam with a fine texture has more lamellae in a given volume of gas and therefore induces more resistance to gas flow. Population-balance models incorporate foam texture explicitly to predict flow properties. A conservation equation for lamellae allows the simulator to track foam texture dynamically, i.e. without the local-equilibrium assumption. The rates of accumulation, convection, generation, and coalescence of foam bubbles are incorporated into the lamella balance, and, if desired, rates of trapping and mobilization as well, as they are for other molecular species in a reservoir simulator.

The transient population balance for the average flowing and trapped lamellae is written as (Chen et al., 2010):

$$\frac{\partial}{\partial t}\left[\phi\left(S_f n_f + S_t n_t\right)\right] + \nabla\cdot\left(u_f n_f\right) = q_f + Q_b \tag{1}$$

where S_f and S_t are flowing and trapped gas saturations, and n_f and n_t are number density of flowing and trapped foam lamellae, respectively. All current models assume $n_f = n_t$ are discussed below. Q_b is a source/sink term, and q_f is the net rate of generation of lamellae which can be defined as

$$q_f = r_g - r_c \tag{2}$$

where r_g and r_c represent generation and coalescence rates, respectively.

The population-balance models can be simplified by assuming local equilibrium if desired (Ettinger and Radke, 1992; Myers and Radke, 2000; Kam and Rossen, 2003; Chen et al., 2010). In the LE

version of the PB models, the rates of foam generation and coalescence are set equal to each other, which defines the LE value of foam texture n_f at each location. Eq. (1) is eliminated from the set of governing equations.

In this section we briefly discuss the models of Chen et al. (2010), Kam et al. (2007), and Kam (2008). The models are summarized in Table (A-2).

The population-balance models examined here use the shear-thinning expression for effective viscosity of Hirasaki and Lawson (1985),

$$\mu_f = \mu_g + \frac{\alpha n_f}{\left|v_f\right|^{1/3}} \tag{3}$$

where μ_g is gas viscosity and μ_f is apparent (effective) gas viscosity in the presence of foam, n_f is the foam lamella density (number of lamella per unit volume), v_f is local gas velocity and α is a proportionality constant that depends on the surfactant formulation and permeability.

2.2.1. Kovscek et al. (1993) model, modified by Chen et al. (2010)

Kovscek et al. (1993) considered Roof snap-off as the mechanism of lamella creation. The model employs a capillary-pressure-dependent kinetic expression for lamella coalescence (to reflect the limiting capillary pressure) and also a term to represent the trapped fraction of foam. The gas relative permeability is then reduced according to the fraction of flowing gas to reflect the effect of gas trapping (Eq. (A-15)). The lamella-generation rate is taken as a power-law expression, proportional to the magnitude of the interstitial velocity of surfactant solution and 1/3 power of the interstitial gas velocity. Chen et al. (2010) introduced an upper limit for the concentration of lamellae that is related to pore size. The upper limit is achieved by the reducing generation rate as this limit is approached; they contended that this accounts for pre-existing gas bubbles that occupy foam-generation sites. They showed that the LE form of this model can predict both low- and high-quality regimes.

2.2.2. Kam et al. model (2007)

Kam et al. (2007) presented a foam model in which lamella creation depends on pressure gradient and also on water saturation or capillary pressure, which governs the presence of lenses or lamellae available to be mobilized (Rossen and Gauglitz, 1990; Gauglitz et al., 2002). Specifically, lamella generation rate is proportional to water saturation and a power-law expression of pressure gradient. In this model, the generation rate monotonically increases with the pressure gradient. Lamella-coalescence rate is a power-law function of (S_w-S_w^*), with the exponent an adjustable parameter. This model can represent multiple (coarse and strong) foam states at the same superficial velocity and jumps between those states, as well as the low- and high-quality regimes for strong foam.

2.2.3. Kam model (2008)

In this extension of the model of Kam et al. (2007), for the lamella creation, the local pressure gradient must exceed the minimum pressure gradient required for lamellae mobilization and division. Kam (2008) proposed a new lamella-creation function, which reaches a plateau at larger pressure gradient (Eq. (A-22)).

3. Corresponding foam model parameters

Parameters S_w^*, *fmdry*, and S_f represent the limiting water saturation in the IT models and the PB models of Kam, while Kovscek et al. and Chen et al. use the corresponding capillary pressure P_c^* in their model. In the STARS model foam weakens in the vicinity of *fmdry* but does not collapse completely at any value of S_w (Farajzadeh et al., 2015). In the UT model, foam collapses in the vicinity of S_w^*, specifically in an interval of ($S_w^* \pm \varepsilon$). In the other models foam collapses completely for $S_w < S_f$, $S_w < S_w^*$, or $P_c > P_c^*$. Parameters R_{ref}, *fmmob* and $(1/F_o)$ represent reference (or maximum) mobility reduction factor that could be achieved by foam when all the conditions are favorable and are directly set in the IT models. Parameters n^* and n_{max} are upper limits for the concentration of foam bubbles in the Chen et al., Kam et al. and Kam models, respectively. They are related to pore size. More than one foam bubble per pore is not expected (Bertin et al. 1998; Kil et al., 2011). Parameters ε, *epdry*, and s_1 control the sharpness of the transition from high-quality to low-quality regimes in the IT models. The extent of the saturation range in the transition from high-quality to low-quality regimes is set to 2ε in the UT model. In both STARS and the Vassenden-Holt models, for the large values of *epdry* and s_1 the transition is sharp and foam collapses within a narrow range of water saturation. In the Kam et al. and Kam models the coalescence exponent n controls the transition, with smaller n giving a sharper transition. The coalescence rate depends on nearness of capillary pressure to P_c^* with an exponent (-2) in the Chen et al. model (Eq.(A-12)). Parameters σ, *epcap* and *a* account for shear-thinning behavior in the low-quality regime in UT, STARS, and modified Vassenden-Holt models, respectively; this would reflect both gas trapping and mobilization and the shear-thinning drag on individual moving bubbles. The population-balance models use the shear-thinning expression by Hirasaki and Lawson (1985) with an exponent of $(-1/3)$ for the dependence of apparent gas viscosity on gas velocity.

4. Fitting foam models to experimental data

In this section we apply different foam models to match the steady-state CO_2 foam experimental data reported by Moradi-Araghi et al. (1997), and the N_2 foam experimental data of Alvarez et al. (2001). Then we discuss and compare the fits with different foam models.

Moradi-Araghi et al. (1997) conducted experiments with CO_2 at 98 °F and 2000 psi in a 551.5-md-permeability reservoir core from the South Cowden Unit in West Texas. The core plugs were 1 inch in diameter and 4.84 inches in length. Foam was made with 2000 ppm surfactant Chaser CD-1050 surfactant in synthetic South Cowden formation brine. The overall pressure drop in the foam experiments was measured and divided by that for single-phase water flow at the same total superficial velocity and reported as the reduction factor (*RF*). Therefore, to calculate the apparent foam viscosity as a function of gas fraction or foam quality (f_g), the reported reduction factor is multiplied by water viscosity (μ_w) at the experimental conditions:

$$\mu_{app}^f = \mu_w RF = 0.65RF \tag{4}$$

where μ_{app}^f is in cp. The *apparent foam viscosity* - μ_{app}^f is defined in Eq. (4) in terms of the total mobility of foam treated as a single phase; the *apparent gas viscosity* μ_f is defined in the foam models above as the effective viscosity *of the gas phase* in foam.

Moradi-Araghi et al. did not report the injection rate in their experiments. Therefore, we assume a total injection rate of 5 ft/day in fitting their experimental data. In a separate study (Farajzadeh et al., 2015), it was found that the choice of flow rate affects only the *MRF or fmmob values* in the UT and STARS models and therefore does alter the ability of the models to fit data.

Alvarez et al. (2001) conducted experiments with N_2 foam at room temperature and 600 psi outlet pressure in 530-md Berea sandstone core. The cores were 2 inches in diameter and 11 inches in length. Foam was made with 1 wt% Bio-Terge AS-40 surfactant in brine of 3 wt% NaCl and 0.01 wt% $CaCl_2$. The pressure gradient at a fixed superficial velocity of 2.5 ft/day was measured and apparent foam viscosity is reported here by multiplication by absolute permeability and dividing by total velocity:

$$\mu_{app}^{f} = \frac{-k\nabla P}{u_w + u_g} \tag{5}$$

Relative-permeability data are not reported for the porous media used in these experiments. Although the parameters depend somewhat on the choice of the relative-permeability parameters (Ma et al., 2014), the generality of our results will not be affected, e.g., with the choice of different relative permeability parameters the correlation between the basic foam properties such as P_c^* and rock properties like permeability will remain unaltered (Farajzadeh et al., 2015). For fitting the foam data we use a relative-permeability function fit to the data of Persoff et al. (1991) in Boise sandstone. We also use the water-gas relative permeability and capillary-pressure functions described in Appendix B. Table 1 summarizes all the rock and fluid properties used in this paper.

The objective function for the optimization of foam model parameters is defined as

$$\Phi(x) = \sum_{i=1}^{n_{data}} \left(\mu_{app_i}^{f}(x) - \mu_{app_i}^{f(\exp)} \right)^2 \tag{6}$$

where x is the vector of foam-model parameters. For example in the STARS model, x = [*fmmob*, *epdary*, *fmdry*, *epcap*]. The reference capillary number, *fmcap*, is not an independent parameter and was set to a fixed value. In Eq. (6) $\mu_{app_i}^{f(\exp)}$ and $\mu_{app_i}^{f}$ are, respectively, the experimental data and values predicted by the foam model for the given set of foam-model parameters. A constrained least-squares algorithm in the optimization toolbox of MATLAB (lsqnonlin function) was used to solve our non-linear data-fitting problem. The constraints are set to physical limits for the foam parameters, e.g. $S_w^* > S_{wc}$, $S_f > S_{wc}$ or *fmdry* > S_{wc} or, depending on the model; and $P_{c@S_{wc}} > P_c^*$.

The final (best-fit) set of fitted parameters may depend on the initial guess. We discuss the issue of non-uniqueness in the various model fits below. In cases where the fit depends on the initial guess, we show here the best fit (i.e., the fit with the smallest value of $\phi(x)$). The model parameters are listed in Tables 2–7 Fig. 2 through 7 show the apparent foam viscosity as a function of foam quality. Symbols are the experimental data and the curves are the match of

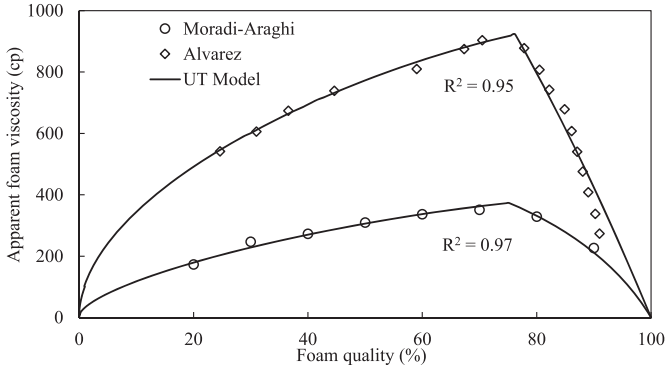

Fig. 2. UT model fit to experimental data using the parameters in Table 2

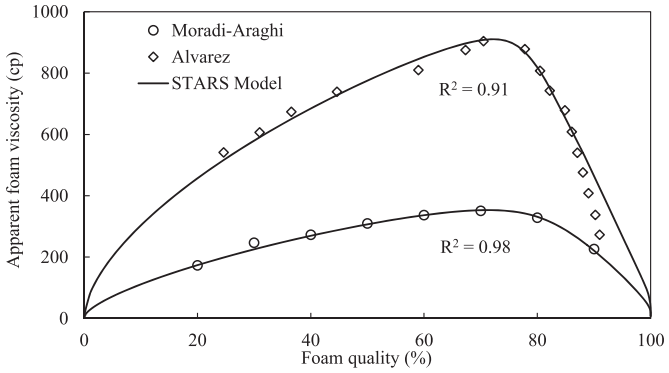

Fig. 3. STARS model fit to experimental data using the parameters in Table 3

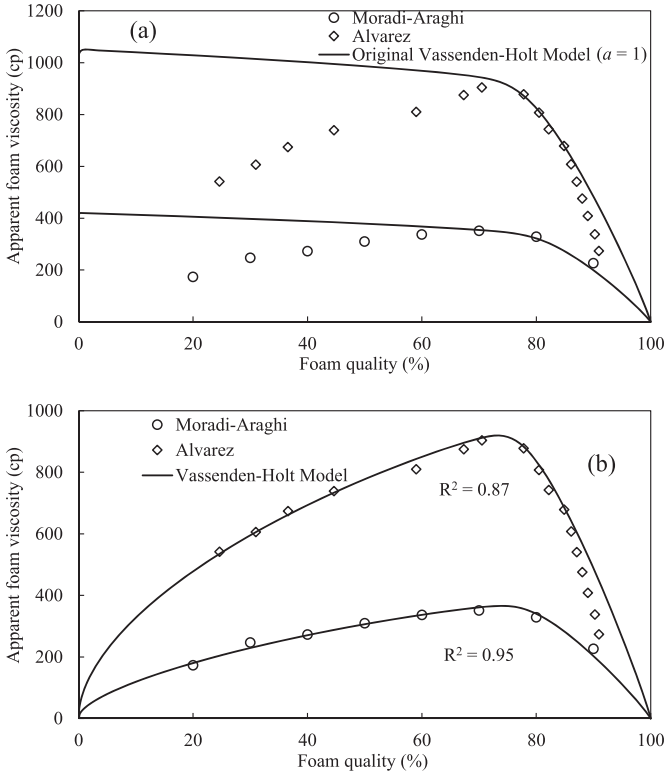

Fig. 4. a) Vassenden-Holt model fit to experimental data using the parameters in Table 4 assuming $a = 1$ (Eq.(A-8)). b) Vassenden-Holt model fit to experimental data using the parameters in Table 4, including *a*.

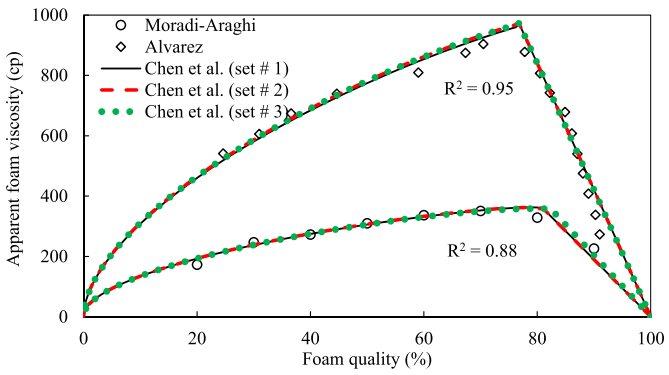

Fig. 5. Chen et al. model fit to experimental data using the parameters in Table 5

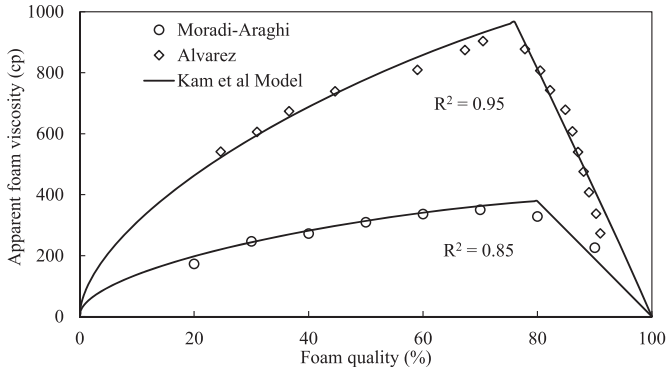

Fig. 6. Kam et al. model fit to experimental data using the parameters in Table 6

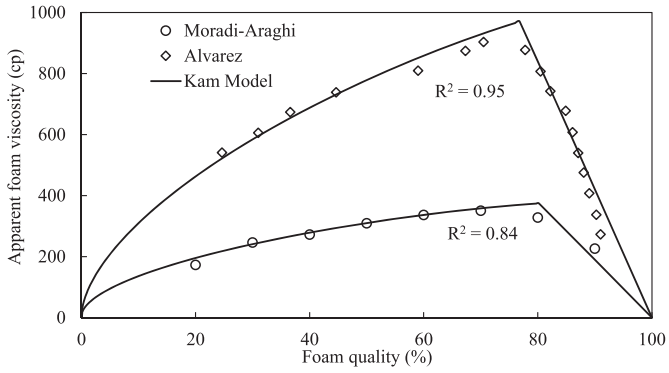

Fig. 7. Kam model fit to experimental data using the parameters in Table 7

the different foam models.

The Vassenden and Holt model was not able to match the data in low-quality regime until we introduced an exponent a for the velocity term (see Eq. (A-8) and Fig. 4). The original model corresponds to a value of the exponent a in Eq. (A-8) of one.

The results show that the two types of models match the experimental data equally well. Some individual models do better in matching the data over some range and others better in other ranges. For instance, for the Moradi-Araghi et al. data the UT and STARS models do a little better than the others.

For the Chen et al. model we match the experimental data using three sets of foam parameters for both the data of Moradi-Araghi et al. and Alvarez et al. (Table 5). In set #1 we assume a maximum gas trapping saturation of 50% and we scale the gas relative permeability along with the gas viscosity to match the experimental results; the resulting fit is shown in Fig. 5. Since the value of trapped-gas saturation is uncertain, in set #2 we ignore gas trapping but we obtain the same quality match by adjusting n^* and slightly adjusting P_c^*. The fits are indistinguishable from each other, as shown in Fig. 5. For at least these two experiments, the trapping parameter in the Chen et al. model does not play an essential part of the data-fitting procedure and could be ignored without harming the fit to the data.

In all the models, except that of Chen et al., the limiting water saturation did not vary with initial guess (though the other parameters did vary). In the Chen et al. model, however, the experimental data could be matched with different values of P_c^* by adjusting parameter k^o_{-1}. In parameter set #1 we use $P_c^* = 0.19$ psi (S_w^*~0.265) and $P_c^* = 0.55$ psi (S_w^*~0.31) for the Moradi-Araghi (CO_2) and Alvarez (N_2) data, respectively. These parameters are compatible with those of other models. In set #2, we had to slightly increase P_c^* to account for trapped-gas saturation. In set #3, we obtained essentially the same fit to the data using $P_c^* = 0.80$ psi for both experiments (S_w^*~0.219 for Moradi-Araghi and S_w^*~0.284 for Alvarez data). There are two implications. First, one cannot derive even an approximate value of P_c^* from these data using Chen et al.'s model without assuming *a priori* a value for the coalescence constant k^o_{-1}. Second, in fitting data to this model, capillary pressure in the foam need not be close to P_c^* in the high-quality or coalescence regime.

Dong (2001) examined this issue in the earlier model of Kovscek et al. (1995). Suppose, as posed in the Introduction, that foam is initially at LE in the high-quality regime, and then gas superficial velocity increases by a factor X. In this model, lamella-generation rate increases by $X^{1/3}$ (Eq. (A-9)). The coalescence rate increases by the factor X (Eq. (A-11)) because of the increase in gas velocity. This increase in coalescence rate does not depend upon nearness to P_c^*. Equilibrium foam texture n_f therefore changes by a factor $(X^{1/3}/X) = X^{-2/3}$. Apparent foam viscosity μ^f_{app} is proportional to $(n_f\, v_g^{-1/3}) \sim (X^{-2/3}X^{-1/3}) = X^{-1}$ because of the dependence on texture and on gas velocity (Eq. (3)). Through Darcy's law on the gas phase, the pressure gradient is proportional to $(v_g\ \mu^f_{app}) \sim (XX^{-1})$, i.e. is constant, with no change in capillary pressure. In this model, the pressure gradient is independent of gas superficial velocity in the high-quality regime because of the particular forms assumed for apparent gas viscosity (Eq. (3)) and the lamella-generation and -coalescence rates, not the divergence of coalescence rate at the limiting capillary pressure.

In the model of Chen et al. (2010) the dependence of generation rate and gas mobility on gas superficial velocity is more complex. In our model fits, the water saturation and capillary pressure in the high-quality regime is the same for all three sets of parameters (#1 to #3) at $S_w = 0.270$–0.274 for Moradi-Araghi and $S_w = 0.311$ for Alvarez et al. Nevertheless, the fitted values of S_w^* and P_c^* vary among the parameter fits to the data: from $S_w^* = 0.265$ to 0.263 to 0.219 (P_c^* between 0.19 and 0.80 psi) for parameter sets #1, 2 and 3, respectively for Moradi-Araghi and $S_w^* = 0.310$ to 0.309 to 0.284 (P_c^* between 0.55 and 0.80 psi) for Alvarez et al. In the model of Chen et al., the high-quality regime water saturation need not be close to S_w^*, nor the capillary pressure close to P_c^*.

The water saturation in the high-quality regime can be derived from the slope of the pressure gradient versus f_g in the experimental data, using Darcy's law for the water phase (Boeije and Rossen, 2013; Ma et al., 2013, 2014). The water saturation in the high-quality regime is calculated to be 0.295 and 0.314 for the Moradi-Araghi and Alvarez data, respectively; the corresponding values of P_c are 0.113 and 0.524 psi. Table 8 summarizes values of S_w^* or the corresponding parameters in other models (*fmdry* in STARS model and S_f in Vassenden-Holt) used to fit the experimental data in different models. While in the UT, STARS, Kam et al., and Kam models the value of S_w^* was close to the water saturation in the high-quality regime, in the Vassenden-Holt and Chen et al. models water saturation in the high-quality regime is not close to S_w^*; nor, is P_c in the foam close to P_c^*.

5. Coalescence function in implicit-texture models

In the IT models examined here foam experiences an abrupt change in its properties near the limiting water saturation. In this section we show that this abrupt change can be expressed by a lamella-destruction function similar to that in population-balance models with a limiting capillary pressure.

The coalescence rate r_c in population-balance models (Eqs. (A-11), (A-20), and (A-23)) can be expressed as

$$r_c = c_c\, n_f f \equiv c_c\, n_f^* n_D f \tag{7}$$

$$f \equiv \frac{r_c}{c_c n_f^* n_D} \tag{8}$$

where c_c is constant, n_f is lamella density (foam texture), n_D is dimensionless foam texture, $n_f^*$is foam texture in the low-quality regime (which we assume to be constant (Alvarez et al., 2001)), and f is a destruction function. In other words, lamellae have a probability of breaking proportional to f, where f can be expressed in terms of water saturation or capillary pressure. Kovscek et al. (1993) suggested that $f \propto (P_c^*\text{-}P_c)^{-2}$; Bertin et al. (1998) proposed $f \propto (P_c^*\text{-}P_c)^{-1}$; Kam et al. (2007) and Kam (2008) assumed $f \propto (S_w\text{-}S_w^*)^{-n}$ with n a fitted parameter. In all the models foam coalescence rate increases sharply at or near the limiting water saturation or the corresponding capillary pressure. Figs. 8 and 9 show the destruction function f used in the PB models in terms of water saturation and capillary pressure. However, there is no theoretical reason nor direct experimental evidence for the choice of one mathematical form of the lamella-destruction function over the others, as long as it increases greatly as P_c approaches P_c^*. We show here that using the mobility-reduction function (specifically the dry-out function) in IT models implies a lamella-destruction function that is similar to the corresponding function in PB models. In other words, the physics of foam collapse near P_c^* is essentially the same in the IT models as in the PB models.

In the UT foam model the gas mobility-reduction factor corresponds to a dimensionless foam lamella density defined by

$$n_D = \begin{cases} 0 & S_w < S_w^* - \varepsilon \\ \left(S_w - S_w^* + \varepsilon\right))/2\varepsilon & S_w^* - \varepsilon \le S_w \le S_w^* + \varepsilon \\ 1 & S_w > S_w^* + \varepsilon \end{cases} \tag{9}$$

where, for water saturations less than S_w^*-ε, foam does not exist ($n_D = 0$). In the high-quality regime, i.e. for S_w^*-$\varepsilon \le S_w \le S_w^* + \varepsilon$, n_D increases linearly with water saturation and reaches its maximum value at $S_w^* + \varepsilon$, where $n_D = 1$. Foam texture remains at its maximum value ($n_D = 1$) through the low-quality regime for $S_w > S_w^* + \varepsilon$.

The Vassenden-Holt model does not imply a fixed maximum foam texture in the low-quality regime. We interpret it in terms of foam texture as follows. The second term in Eq. (A-8) corresponds to mobility in the low-quality regime. We interpret the $(u_g/u_{go})^a$ term as reflecting non-Newtonian viscosity or gas trapping, but not changing foam texture, in this regime. We use texture in the limit

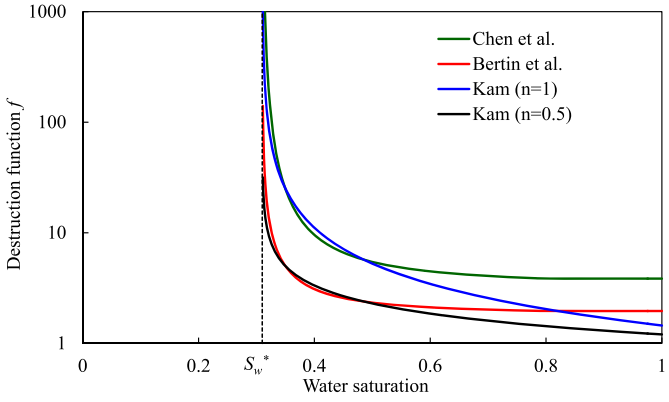

Fig. 8. Lamella-destruction function f in different population-balance models plotted as a function of water saturation. The vertical dotted line represents S_w^*.

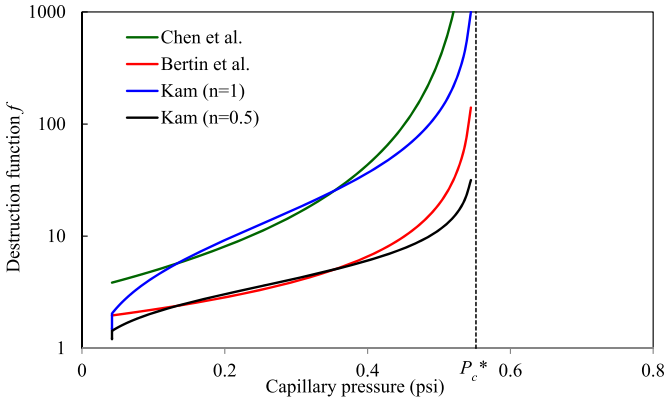

Fig. 9. Lamella-destruction function f in different population-balance models plotted as a function of capillary pressure. The vertical dotted line represents P_c^*.

$S_w \to 1$ as the reference texture. Let F' be the function F defined in Eq. (A-8) but without the (u_g/u_{go}) term. Then

$$F'(S_w) = \exp\left[\left(S_f - S_w\right)S_1\right] + F_o \exp\left[\left(S_f - S_w\right)S_2\right] \tag{10}$$

This function, related to the mobility-reduction factor F in Vassenden-Holt model, is inversely proportional to foam texture. Thus

$$n_D = \left(\frac{1}{F'(S_w)} - 1\right)\left(\frac{1}{F'(1)} - 1\right)^{-1} \tag{11}$$

In the STARS model, gas mobility reduction is proportional to FM, with the maximum reduction when $FM = 1/(1 + fmmob)$. Excluding the shear-thinning effect (F_5 function) from FM, the corresponding dimensionless foam texture is defined by

$$n_D = \frac{1 + fmmob.F_2}{1 + fmmob} \tag{12}$$

Different population-balance models use different lamella-generation functions, and the best choice for this function remains controversial. Kam and Rossen (2003) show that different lamella-generation functions can give the same steady-state foam behavior. Moreover, behavior in the coalescence regime is dominated by an abrupt increase in coalescence rate, not a change in generation rate. Therefore, for simplicity, we assume here a constant bubble-generation rate, r_g. Zitha (2006) assumes a constant generation rate in his model. More complicated generation functions could be used without changing our conclusions, which hinge on abrupt changes in foam behavior near P_c^* or S_w^*. Therefore, assuming local equilibrium, the destruction function is

$$f = \frac{r_g}{c_c\, n_D n_f^*} = \frac{r_{gD}}{n_D} \tag{13}$$

with

$$r_{gD} \equiv \frac{r_g}{c_c\, n_f^*} \tag{14}$$

Fig. 10 through 15 show the lamella-destruction functions implied by the UT, STARS, and Vassenden-Holt models, using the parameter values fit to the experimental data of Moradi-Araghi et al. and Alvarez et al. in Figs. 2, 3 and 4b. The UT model implies a destruction function that remains constant in the low-quality regime and increases sharply in the interval $S_w^* \pm \varepsilon$, diverging to

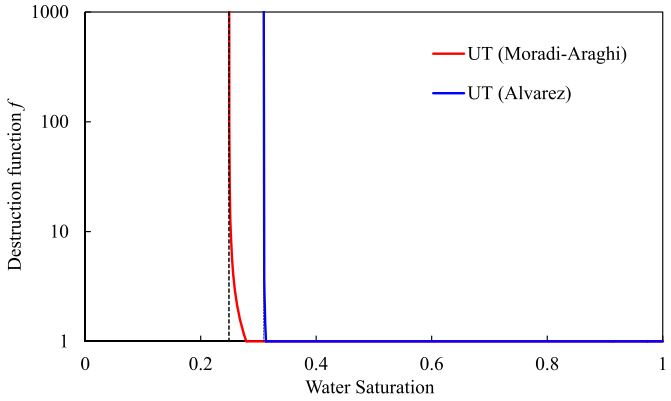

Fig. 10. Lamella-destruction function f implied by the UT foam model plotted as a function of water saturation. The vertical dotted lines represent (S_w^*- ε).

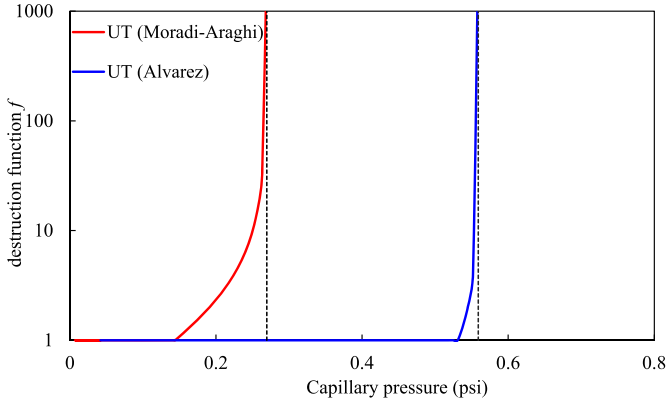

Fig. 11. Lamella-destruction function f implied by the UT foam model plotted as a function of capillary pressure. The vertical dotted lines represent the capillary pressure at (S_w^*- ε).

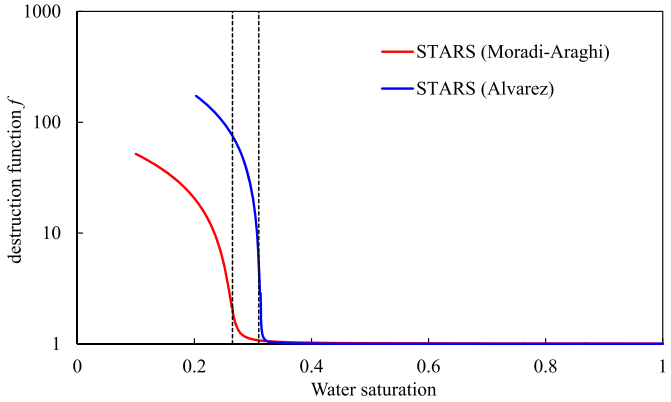

Fig. 12. Lamella-destruction function f implied by the STARS foam model plotted as a function of water saturation. The vertical dotted lines represent *fmdry*.

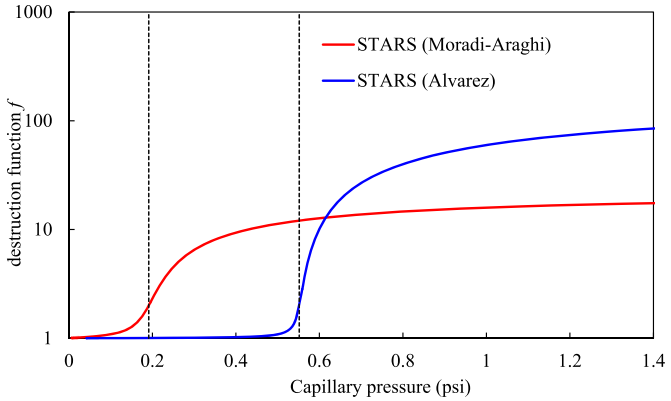

Fig. 13. Lamella-destruction function f implied by the STARS foam model plotted as a function of capillary pressure. The vertical dotted lines represent capillary pressure at *fmdry*.

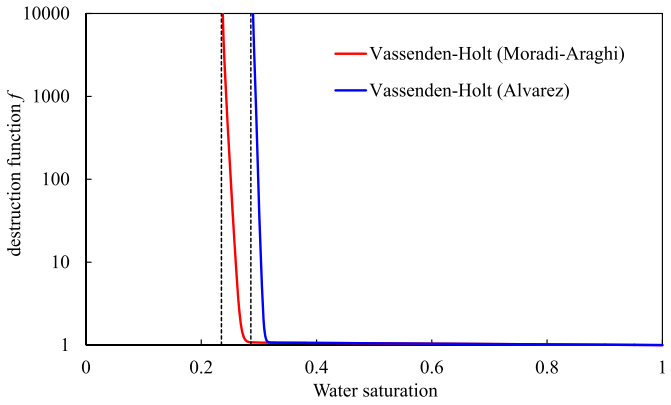

Fig. 14. Lamella-destruction function f implied by the Vassenden-Holt foam model plotted as a function of water saturation. The vertical dotted lines represent S_f.

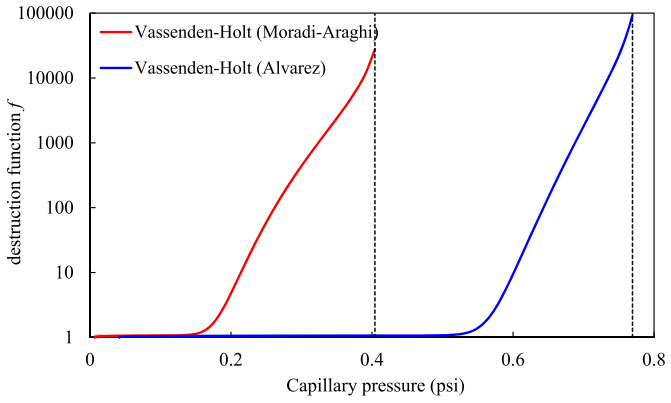

Fig. 15. Lamella-destruction function f implied by the Vassenden-Holt foam model plotted as a function of capillary pressure. The vertical dotted lines represent the capillary pressure at S_f.

infinity at S_w^*-ε. In the Vassenden-Holt model the destruction function increases sharply in the high-quality regime and it reaches its maximum value at S_f. In this model the destruction function increases with larger slope for a larger value of s_1. The STARS model implies a destruction function that increases sharply in the vicinity of *fmdry* but remains finite at all water saturations. In this model, the destruction function increases more abruptly as S_w approaches *fmdry* for larger values of *epdry*. The lamella-destruction functions implied by these IT models are similar to those in the PB models. There is no theoretical reason or experimental justification to prefer any of the functions in Figs. 9, 11 and 13, or 15 above the others. Thus, in terms of the most important mechanism in foam behavior without oil (Farajzadeh et al., 2012), i.e. foam collapse at the limiting capillary pressure, the IT models are as well-supported by theory and experiment as the population-balance models.

Fig. 16 through 19 show dimensionless foam texture in the implicit-texture and population-balance models, using the parameter values fit to Moradi-Araghi et al. and Alvarez et al. experimental data. In the population-balance models, dimensionless foam texture is defined as the foam bubble density (n_f) divided by the maximum foam bubble density in the low-quality regime n_{max} ($n_D = n_f/n_{max}$). In all the models, dimensionless foam texture drops sharply close to S_w^*. Dimensionless foam textures implied in the IT models are similar to those in population-balance models.

6. Summary and conclusions

Implicit-texture (IT) models are often perceived as not reflecting the essential physics of foam in porous media. Although only population-balance models can represent the entrance region, dynamics at shock fronts, the process of foam generation, and regions in heterogeneous or fractured media, where abrupt heterogeneities mean that foam is not at local equilibrium, in this study we focus on the ability to fit steady-state data. IT models all assume local equilibrium (LE). Therefore, we compare IT and LE version of population-balance (PB) models. The main conclusions are as follows:

- An essential test of a model's usefulness is its ability to match available data and thereby give confidence in predicting new data. We show that both IT models and PB models at LE match the steady-state experimental data for CO_2 and N_2 foam presented here equally well. The corresponding parameters of the different foam models are presented and discussed.
- The original Vassenden-Holt model does not match the data in low-quality regime until we introduce an exponent a in the velocity term.
- The trapping parameter in the Chen et al. model does not play an essential part of the data-fitting procedure, for these data, at least.
- In the Vassenden-Holt and Chen et al. models, the high-quality or coalescence regime does not necessarily reflect a capillary pressure near the limiting capillary pressure (P_c^*). Values of P_c^* fit to foam-mobility data with model of Chen et al. are sensitive to the value of the coalescence kinetic parameter k_{-1}^o.
- We define dimensionless foam texture implicit in the IT models and derive the foam-coalescence-rate function implicit in these models. The results show that the IT models that incorporate an abrupt change in foam properties near a given water saturation can be recast as LE versions of corresponding population-balance models with a lamella-destruction function similar to those in current PB models. The trends in dimensionless foam texture implicit in the IT models is similar to that in the PB models. In other words, both types of models, at least in the LE approximation and without oil, equally honor the physics of foam behavior in porous media.

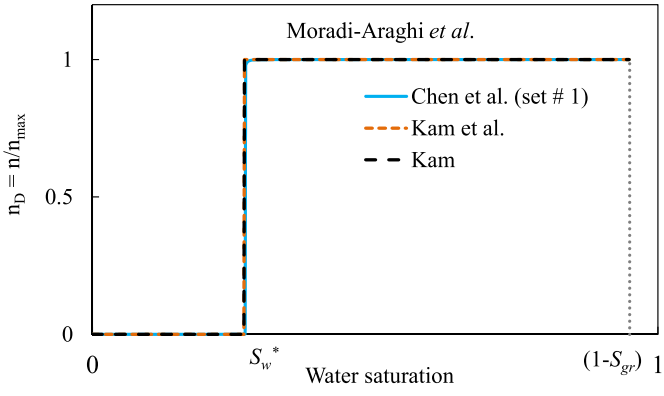

Fig. 16. Dimensionless foam texture obtained in the population-balance models to fit to Moradi-Araghi et al. data.

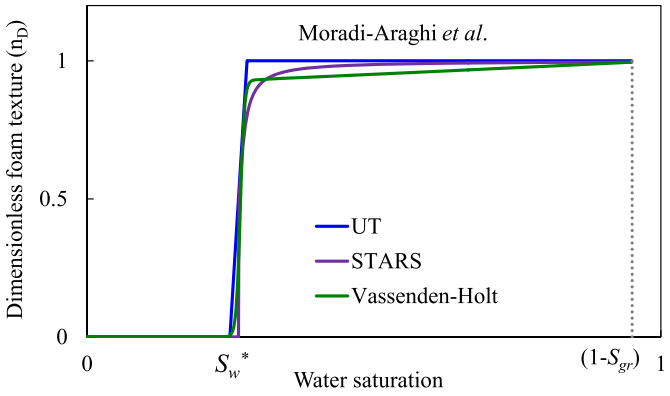

Fig. 17. Dimensionless foam texture implied by implicit-texture models to fit to Moradi-Araghi et al. data.

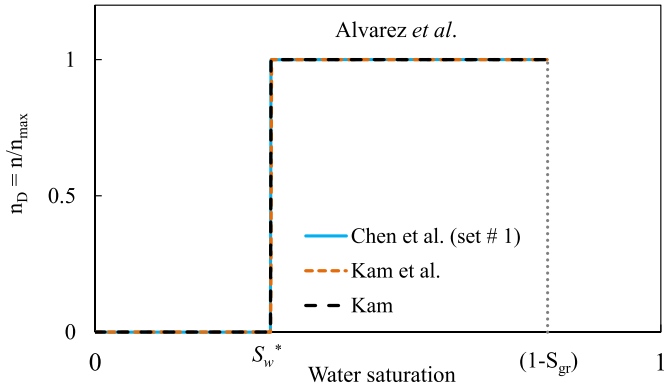

Fig. 18. Dimensionless foam texture obtained in population-balance models to fit to Alvarez et al. data.

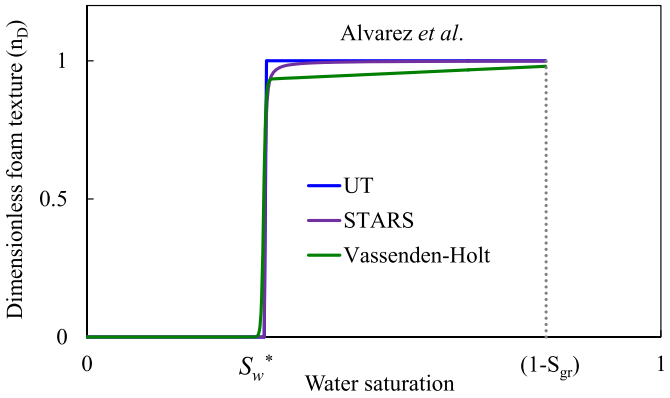

Fig. 19. Dimensionless foam texture implied by implicit-texture models to fit to Alvarez et al. data.

Acknowledgement

The authors thank Prof. C. van Kruijsdijk and Dr S. Vincent-Bonnieu for careful review of the manuscript. They also thank

Shell Global Solutions International for permission to publish this work.

Nomenclature

a	shear-thinning exponent in Vassenden-Holt model
b	capillary pressure model parameters
c_c	coalescence rate constant
c_g	generation rate constant in Kam et al. and Kam model
C_s	surfactant concentration
C_s^*	threshold surfactant concentration in UT model
C_s^o	reference surfactant concentration in Chen et al. model
epcap	shear-thinning exponent in STARS model
epdry	factor governing abruptness of dry-out calculation (F_2) in STARS model
F	foam mobility multiplier in Vassenden- Holt model
f	destruction function
F'	function in Vassenden-Holt model reflecting foam texture but non-Newtonian effects
F_2	dry-out function in STARS model
F_5	shear-thinning function in STARS model
FM	mobility reduction factor in STARS model
fmcap	reference rheology capillary number in STARS model
fmdry	reference water saturation in dry-out calculation (F_2) in STARS model
fmmob	maximum resistance factor in STARS model
F_o	foam mobility constant in Vassenden-Holt model
k	Permeability
k_1	generation rate coefficient in Chen *et a*l. model
k_{-1}	coalescence coefficient in Chen et al. model
k_1^o	model parameter in Chen et al. model
k_{-1}^o	model parameter in Chen et al. model
k_{rg}	gas relative permeability in absence of foam
k_{rg}^f	gas relative permeability in presence of foam
k_{rg}^o	gas endpoint relative permeability
m	model parameter Kam et al. Model
n	coalescence exponent in Kam et al. and Kam model
n^*	limiting (maximum) lamella density in Chen et al. model
N_{ca}	capillary number
n_D	dimensionless lamella density
n_f	number density of lamellae (lamellae/volume gas)
n_f^*	reference lamella density used in definition of n_D
n_g	gas exponent relative permeability
n_{max}	Maximum foam lamella density in Kam model
n_t	number density of trapped foam bubbles
n_w	water exponent relative permeability
P_c	capillary pressure
P_c^*	limiting capillary pressure
P_{ce}	entry capillary pressure
P_{cmax}	limiting value of P_c^* in Chen et al. model
Q_b	source/sink term for foam bubbles
q_f	net rate of generation of foam bubbles
R	foam resistance factor in UT model
r_c	foam coalescence rate
RF	mobility reduction factor
r_g	foam generation rate
r_{gD}	dimensionless foam generation rate
R_{ref}	reference foam resistance factor at reference gas velocity in UT model
s_1	slope of the gas relative permeability at high quality regime in Vassenden-Holt model
s_2	slope of the gas relative permeability at low quality regime in Vassenden-Holt model
S_f	flowing gas saturation (lowest water saturation) for foam effect in Vassenden-Holt model
S_{fD}	dimensionless gas saturation in the presence of foam
S_{gD}	dimensionless gas saturation
S_t	trapped gas saturation
S_w	water saturation
S_w^*	limiting water saturation
S_{wc}	connate water saturation
S_{wD}	dimensionless water saturation
u_f	Darcy velocity of gas in foam
u_g	gas Darcy velocity
u_{gref}	reference gas Darcy velocity
u_w	water Darcy velocity
v_f	local gas velocity
v_w	local water velocity
x	vector of foam model parameters
X_t	trapping foam fraction Chen et al. model
$X_{t,max}$	maximum trapping fraction in Chen et al. model
α	proportionality constant
β	trapping parameter Chen et al. model
ε	width of high-quality regime in UT model (in terms of S_w)
λ	capillary pressure model parameters
μ_f	apparent gas viscosity (effective viscosity of gas phase in foam)
μ_f^{app}	apparent foam viscosity, treated as a single phase
μ_g	gas viscosity in the absence of foam
σ	power-low exponent in UT model
σ_{co2}	CO_2-water surface tension
σ_{N2}	N_2-water surface tension
Φ	objective function for the optimization of foam model
ω	constant exponent in Chen et al. Model
∇P	pressure gradient
∇P_o	model parameters related to minimum pressure gradient in Kam model

Appendix A. Foam Models

Table (A-1)
IT foam models used in this study

Model description	Model parameters
UT Model (1994) $$k_{rg}^f = \begin{cases} k_{rg} & S_w < S_w^* - \varepsilon \ \text{or} \ C_S < C_S^* \\ \dfrac{k_{rg}}{\left(1 + \left((R-1)\left(S_w - S_w^* + \varepsilon\right)\right)/2\varepsilon\right)} & S_w^* - \varepsilon \le S_w \le S_w^* + \varepsilon \ \&\ C_S \ge C_S^* \\ k_{rg}^f = \dfrac{k_{rg}}{R} & S_w > S_w^* + \varepsilon \ \&\ C_S \ge C_S^* \end{cases} \quad \text{(A-1)}$$	k_{rg}: gas relative permeability k_{rg}^f: foam relative permeability C_s: surfactant concentration C_s^*: threshold surfactant conc. S_w^*: limiting water saturation u_g: gas Darcy velocity u_{gref}: ref. gas Darcy velocity R: foam resistance factor ε: Water saturation tolerance

(*continued on next page*)

Table (A-1) (*continued*)

Model description		Model parameters
$R = R_{ref}\left(\frac{u_g}{u_{g_{ref}}}\right)^{\sigma-1}$	(A-2)	σ: power-low exponent σ = 1, Newtonian σ < 1, shear-thinning
STARS Model		*FM*: mobility reduction factor
$k_{rg}^f = k_{rg} \times FM$	(A-3)	*fmmob*: max. reduction factor
$FM = \frac{1}{1 + fmmob(F_1 \times F_2 \times F_3 \times F_4 \times F_5 \times F_6)}$	(A-4)	F_2:dry-out function
$F_2 = 0.5 + \frac{1}{\pi}\arctan(epdry(S_w - fmdry))$	(A-5)	F_5: shear thinning function *epdry*: ref. dry-out slop in dimensionless dryout calculation
$F_5 = \begin{cases} \left(\frac{fmcap}{N_{ca}}\right)^{epcap} & N_{ca} > fmcap \\ 1 \quad N_{ca} \le fmcap \end{cases}$	(A-6)	*fmdry*: dry-out factor N_{ca}: capillary number *fmcap*: ref. rheology capillary number *epcap*: shear-thinning exponent
Vassenden-Holt Model		u_g: gas Darcy velocity
$k_{rg}^f = k_{rg} \times F$	(A-7)	u_{go}: ref. gas Darcy velocity *F*: foam mobility multiplier
$F = \begin{cases} e^{(S_f - S_w)s_1} + \left(\frac{u_g}{u_{go}}\right)^a F_o e^{(S_f - S_w)s_2} & S_w > S_f \\ 1 & S_w \le S_f \end{cases}$	(A-8)	F_o: foam mobility multiplier at ref. gas velocity S_f: lowest water saturation for foam effect s_1: slop of the gas relative permeability at high quality regime s_2: slop of the gas relative permeability at low quality regime *a*: shear thinning exponent (for original model $a = 1$)

Note: In the most recent version of STARS, the parameter *fmdry* is renamed *sfdry*, and *epdry* is renamed *sfbet* (Coombe, 2012). The water saturation around which foam collapses (*fmdry*) is no longer treated as a constant, but is a function of surfactant concentration, oil saturation, salt concentration, and capillary number. If one disables these other functionalities *sfdry* plays the same roll as *fmdry* as described here.

Table (A-2)
Population-balance foam models used in this study

Model description		Model Parameters
Chen et al. (2010)		v_f: local gas velocity v_w: local water velocity
– generation rate $r_g = k_1\left\lvert\overrightarrow{v_w}\right\rvert\left\lvert\overrightarrow{v_f}\right\rvert^{1/3}$	(A-9)	k_1: generation coefficient
$k_1 = k_1^o\left[1 - \left(n_f/n^*\right)^{\omega}\right]$	(A-10)	k_1^o: model parameter (const.)
– coalescence rate $r_c = k_{-1}\left\lvert\overrightarrow{v}_f\right\rvert n_f$	(A-11)	n_f: flowing foam lamella density n^*: limiting (max) lamella density
$k_{-1} = k_{-1}^o\left(\frac{P_c}{P_c^* - P_c}\right)^2$	(A-12)	ω: constant exponent k_{-1}: coalescence coefficient
$P_c^* = P_{c,\max}^* \tanh(C_s/C_s^o)$	(A-13)	k_1^o: model parameter (const.) P_c:capillary pressure
– at LE $n_f^{\omega} + \frac{n^{*\omega}k_{-1}\left\lvert v_f\right\rvert^{2/3}}{k_1^o\lvert v_w\rvert}n_f - n^{*\omega} = 0$	(A-14)	P_c^*: limiting capillary pressure $P_{c,max}^*$: limiting value of P_c^*
– foam relative permeability $k_{rg}^f = k_{rg}^o\left(S_{f_D}\right)^{n_g}$	(A-15)	C_s: surfactant concentration
$S_{f_D} = S_{g_D}(1 - X_t)$	(A-16)	C_s^o: ref. surfactant concentration
$X_t = X_{t,\max}\left(\frac{\beta n_t}{1 + \beta n_t}\right)$	(A-17)	k_{rg}^o: gas endpoint relative permeability n_g: gas exponent relative permeability
– at LE $n_t = n_f$	(A-18)	S_{gD}: dimensionless gas saturation S_{fD}: dimensionless gas saturation in presence of foam X_t: trapping foam fraction $X_{t,max}$: maximum trapping foam fraction n_t: trapped foam lamella density β: trapping parameter
Kam et al. (2007)		n_f: foam lamella density
generation rate $r_g = c_g S_w(\nabla p)^m$	(A-19)	c_g: generation rate coefficient c_c: coalescence rate coefficient
– coalescence rate $r_c = c_c n_f\left(\frac{1}{S_w - S_w^*}\right)^n$	(A-20)	S_w^*: limiting water saturation ∇P: pressure gradient
– at LE $n_f = \begin{cases} n_f = \frac{c_g}{c_c}S_w\left(S_w - S_w^*\right)^n(\nabla P)^m & n_f < n_{\max} \\ n_{\max} & n_f \ge n_{\max} \end{cases}$	(A-21)	*n*: coalescence exponent *m*: model parameter
Kam (2008)		n_f: foam lamella density
– generation rate $r_g = \frac{c_g}{2}\left(erf\left(\frac{\nabla P - \nabla P_o}{\sqrt{2}}\right) - erf\left(\frac{-\nabla P_o}{\sqrt{2}}\right)\right)$	(A-22)	c_g: generation rate coefficient c_c: coalescence rate coefficient
– coalescence rate $r_c = c_c n_f\left(\frac{S_w}{S_w - S_w^*}\right)^n$	(A-23)	S_w^*: limiting water saturation ∇P: pressure gradient
– at LE $n_f = \begin{cases} \frac{c_g}{2c_c}\left(\frac{S_w - S_w^*}{S_w}\right)^n\left(erf\left(\frac{\nabla P - \nabla P_o}{\sqrt{2}}\right) - erf\left(\frac{-\nabla P_o}{\sqrt{2}}\right)\right) & n_f < n_{\max} \\ n_{\max} & n_f \ge n_{\max} \end{cases}$	(A-24)	∇P_o: model parameters related to minimum pressure gradient *n*: coalescence exponent n_{max}: maximum lamella density

Table 1
Rock and fluid properties

Parameters	Moradi-Araghi et al.	Alvarez et al.
gas	CO_2	N_2
$k\,(md)$	551.5	530
$u_t\,(ft/day)$	5	2.5
$\mu_w\,(cp)$	0.65	0.7
$\mu_g\,(cp)$	0.05	0.02
S_{wr}	0.1	0.2
S_{gr}	0.05	0.2
k°_{rw}	0.22	0.2
k°_{rg}	1.0	0.94
n_w	4	4.2
n_g	1.83	1.3

Table 2
UT model parameters to fit experimental data

Parameters	Moradi-Araghi et al.	Alvarez et al.
R_{ref}	8.4×10^3	5.6×10^4
S^*_w	0.264	0.31
ε	0.015	0.002
$u_{g_{ref}}\,(ft/day)$	1.0	1.0
σ	0.8	0.6

Table 3
STARS model parameters to fit experimental data

Parameters	Moradi-Araghi et al.	Alvarez et al.
fmmob	1.58×10^4	1.6×10^5
fmdry	0.265	0.31
epdry	100	500
fmcap[a]	2.46×10^{-5}	2.46×10^{-5}
epcap	0.2	0.5

[a] *fmcap* is a reference capillary pressure below which shear-thinning is assumed not to apply. The choice of this reference also affects the value of *fmmob* (Boeije and Rossen, 2013).

Table 4
Vassenden-Holt (1998) model parameters to fit experimental data

Parameters	Moradi-Araghi et al.		Alvarez et al.	
	Original Model ($a = 1$)	Modified Model	Original Model ($a = 1$)	Modified Model
F_o	4.5×10^{-5}	1.2×10^{-4}	1.23×10^{-5}	1.8×10^{-5}
S_f	0.235	0.235	0.286	0.286
s_1	280	280	500	500
s_2	0.1	0.1	0.1	0.1
u_{g_o}	1.0	1.0	1.0	1.0
a	1.0	0.2	1.0	0.35

Table 5
Chen et al. (2010) model parameters to fit experimental data

Parameters	Moradi-Araghi et al.			Alvarez et al.		
	Set# 1	Set# 2	Set# 3	Set# 1	Set# 2	Set# 3
$k^o_1\,(ft^{-13/3}day)$	8×10^{15}	8×10^{15}	8×10^{15}	9×10^{18}	9×10^{18}	9×10^{18}
$k^o_{-1}\,(ft^{-1})$	30	30	1.5×10^4	20	20	3×10^4
$n^*\,(ft^{-3})$	5.4×10^{11}	1.9×10^{12}	1.9×10^{12}	5.4×10^{11}	1.34×10^{12}	1.34×10^{12}
$P^*_c\,(psi)$	0.19	0.20	0.8	0.55	0.555	0.8
$X_{t,max}$	0.5	0	0	0.5	0	0
β	1×10^{-9}	–	–	1×10^{-9}	–	–
$\alpha(ft^{10/3}day^{-1/3}cp)$	5×10^{-10}	5×10^{-10}	5×10^{-10}	1.7×10^{-9}	1.7×10^{-9}	1.7×10^{-9}

Table 6
Kam et al. (2007) model parameters to fit experimental data

Parameters	Moradi-Araghi et al.	Alvarez et al.
c_g/c_c	8×10^{16}	8×10^{16}
S^*_w	0.268	0.31
n	2.05	1.91
m	0.7	0.2
$n_{\max}\,(ft^{-3})$	5.4×10^{11}	5.4×10^{11}
$\alpha(ft^{10/3}day^{-1/3}cp)$	1.83×10^{-9}	4.2×10^{-9}

Table 7
Kam (2008) model parameters to fit experimental data

Parameters	Moradi-Araghi et al.	Alvarez et al.
$c_g/2c_c$	2.3×10^{15}	2.3×10^{15}
S^*_w	0.268	0.31
n	1.83	1.64
$\nabla P_o\,(psi)$	0.01	0.01
$n_{\max}\,(ft^{-3})$	5.4×10^{11}	5.4×10^{11}
$\alpha(ft^{10/3}day^{-1/3}cp)$	4.57×10^{-13}	4.2×10^{-9}

Appendix B. Relative-Permeability and Capillary-Pressure Models Used in This Study

Two-phase foam-free water-gas relative permeabilities are calculated from the following expressions

$$k_{rw} = k^o_{rw}(S_{wD})^{n_w} \tag{B-1}$$

$$k_{rg} = k^o_{rg}(1 - S_{wD})^{n_g} \tag{B-2}$$

where S_{wD} is dimensionless water saturation and is defined as

$$S_{wD} = \frac{S_w - S_{wr}}{1 - S_{wr} - S_{gr}} \tag{B-3}$$

The general form of gas-water capillary pressure represented by Li (2004) is

$$P_c = P_{c@S_{wc}}(1 - bS_{wD})^{-1/\lambda} \tag{B-4}$$

where, $P_{c@Swc}$ is the capillary pressure at the connate water saturation, S_{wc}, when drainage capillary pressure is used. b and λ are constants and are defined as

Table 8
Values of limiting water saturation used in different models

Model	S_w^* (Moradi-Araghi)	S_w^* (Alvarez et al.)
UT	0.264	0.31
STARS	0.265	0.31
Vassenden-Holt	0.235	0.286
Chen et al.	0.265–0.219	0.310–0.284
Kam et al.	0.268	0.31
Kam	0.268	0.31

$$n_w = 1 + \frac{2}{\lambda} \tag{B-5}$$

$$b = 1 - \left(\frac{P_{ce}}{P_{c@Swc}}\right)^{-\lambda} \tag{B-6}$$

where n_w is the water Corey exponent and P_{ce} is the capillary entry pressure.

Parameters $P_{c@Swc}$ and P_{ce} are assumed here to be 21.036 and 0.042 *psi* for the data of Alvarez et al.for foam made with N_2. Assuming a similar rock type the capillary pressure for the Moradi-Araghi et al. (CO_2) data set can be scaled as

$$P_{C_{CO_2}} = P_{C_{N_2}} \frac{\sigma_{CO_2}}{\sigma_{N_2}} \tag{B-7}$$

where σ_{CO2}(~5 dyne/cm) and σ_{N2}(~30 dyne/cm) are CO_2 and N_2 interfacial tension with water, respectively. Figure (B-1) shows the capillary-pressure curves used in this study to model CO_2 and N_2 experiments.

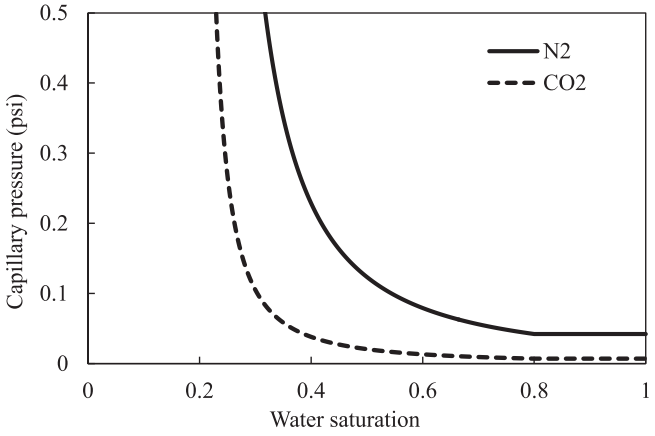

Fig. (B-1). Capillary-pressure curves used to model CO_2 (Moradi-Araghi) and N_2 (Alvarez et al.) experiments.

References

Alvarez, J., Rivas, H., Rossen, W.R., 2001. Unified model for steady-state foam behavior at high and low foam qualities. SPEJ 6 (03), 325–333. SPE-74141-PA.

Andrianov, A., Farajzadeh, R., Mahamoodi Nick, M., Talanana, M., Zitha, P.L.J., 2012. Immiscible foam for enhancing oil recovery: bulk and porous media experiments. Ind. Eng. Chem. Res. 51 (5), 2214–2226.

Aronson, Radke, C.J., 1994. The influence of disjoining pressure on foam stability and flow in porous Media. Colloids Surfaces A Physicochem. Eng. Aspects 83 (2), 109–120.

Bernard, G.G., Holm, L.W., 1964. Effect of foam on permeability of porous Media to Gas. SPEJ 4 (03), 267–274. SPE-983-PA.

Bernard, G.G., Holm, L.W., Jacobs, W.L., 1965. Effect of foam on trapped Gas saturation and on permeability of porous Media to water. SPEJ 5 (04), 195–300. SPE-1204-PA.

Bertin, H.J., Quintard, M.Y., Castanier, L.M., 1998. Modeling transient foam flow in porous Media using a bubble population correlation. SPEJ 3 (04), 356–362. SPE-49020 PA.

Boeije, C.S., Rossen, W.R., 2013. Fitting foam simulation model parameters to data. In: Presented at the 17th European Symposium on Improved Oil Recovery, St. Petersburg, Russia, 16–18 April.

Chen, Q., Gerritsen, M.G., Kovscek, A.R., 2010. Modeling foam displacement with the local-equilibrium approximation: theory and experimental verification. SPEJ 15 (01), 171–183. SPE-116735-PA.

Cheng, L., Reme, A.B., Shan, D., Coombe, D.A., Rossen, W.R., 2000. Simulating foam processes at high and low foam qualities. In: Paper SPE 59278 Presented at the SPE/DOE Improved Oil Recovery Symposium, Tulsa, OK, 3–5 April.

Computer Modeling Group, 2012. STARS User's Manual.

Coombe, D.A., 2012. Personal Communication.

de Vries, A.S., Wit, K., 1990. Rheology of Gas/Water foam in the quality range relevant to steam foam. SPE Reserv. Eng. 5 (02), 185–192. SPE-18075-PA.

Delshad, M., Wheeler, M.F., Sepehrnoori, K., 2013. UTDOE-CO2 CO2 Flooding Reservoir Simulator, U.S. Department of Energy. DOE under Contract Number DE-FE0005952.

Delshad, 2013. The University of Texas Chemical Flooding Simulator. UTCHEM. The University of Texas at Austin. http://www.cpge.utexas.edu/?q=UTChem_GI.

Dong, Y., 2001. Experimental Study of CO_2 Foam Flow in Porous Media and Application of Fractional-flow Method to Foam Flow. MS thesis. Department of Petroleum and Geosystems Engineering, The University of Texas at Austin.

Ettinger, R.A., Radke, C.J., 1992. Influence of texture on steady foam flow in Berea Sandstone. SPE Reserv. Eng. 7 (01), 83–90. SPE-19688-PA.

Falls, A.H., Hirasaki, G.J., Patzek, T.W., Gauglitz, D.A., Miller, D.D., Ratulowski, J., 1988. Development of a mechanistic foam simulator: the population balance and generation by snap-off. SPE Reserv. Eng. 3 (03), 884–892. SPE-14961-PA.

Falls, A.H., Musters, J.J., Ratulowski, J., 1989. The apparent viscosity of foams in homogeneous bead packs. SPE Reserv. Eng. 4 (2), 155–164. SPE-16048-PA.

Farajzadeh, R., Andrianov, A., Krastev, R., Hirasaki, G.J., Rossen, W.R., 2012. Foam–oil interaction in porous media: implications for foam assisted enhanced oil recovery. Adv. colloid interface Sci. 183–184, 1–13.

Farajzadeh, R., Lotfollahi, Eftekhari, A.A.,C., Rossen, W.R., Hirasaki, G.J.H., 2015. Effect of permeability on implicit-texture foam model parameters and the limiting capillary pressure. Energy & fuels 29 (5), 3011–3018.

Farajzadeh, R., Muruganathan, R.M., Rossen, W.R., Krastev, R., 2011. Effect of Gas type on foam film permeability and its implications for foam flow in porous Media. Adv. Colloid Interface Sci. 168, 1–2, 71–78.

Friedmann, F., Chen, W.H., Gauglitz, P.A., 1991. Experimental and simulation study of high-temperature foam displacement in porous Media. SPE Reserv. Eng. 6 (01), 37–45.

Gauglitz, P.A., Friedmann, F., Kam, S.I., Rossen, W.R., 2002. Foam generation in homogeneous porous Media. Chem. Eng. Sci. 57 (19), 4037–4052.

Hirasaki, G.J., Lawson, J.B., 1985. Mechanisms of foam flow in porous Media: apparent viscosity in smooth capillaries. SPEJ 25 (02), 176–190. SPE-12129-PA.

Kam, S.I., Rossen, W.R., 2003. A model for foam generation in homogeneous porous Media. SPEJ 8 (4), 417–425. SPE-87334-PA.

Kam, S.I., 2008. Improved mechanistic foam simulation with foam catastrophe theory. Colloids Surfaces A Physicochem. Eng. Aspects. 318, 1–3, 62-77.

Kam, S.I., Nguyen, Q.P., Li, Q., Rossen, W.R., 2007. Dynamic simulations with an improved model for foam generation. SPEJ 12 (1), 35–48. SPE-90938-PA.

Khatib, Z.I., Hirasaki, G.J., Falls, A.H., 1988. Effects of capillary pressure on coalescence and phase mobilities in foams flowing through porous Media. SPE Reserv. Eng. 3 (03), 919–926. SPE 15442-PA.

Kil, R.A., Nguyen, Q.P., Rossen, W.R., 2011. Determining trapped Gas in foam from ct images. SPE J. 16, 24–34.

Kovscek, A.R., Patzek, T.W., Radke, C.J., 1993. Simulation of foam transport in porous media. SPE 26402, Presented at SPE Annual Technical Conference and Exhibition, Houston, Texas, pp. 3–6. October.

Kovscek, A.R., Radke, C.J., 1994. Fundamentals of foam transport in porous Media. In: Schramm, L. (Ed.), Foams: Fundamentals and Applications in the Petroleum Industry, ACS Symposium Series, No. 242. American Chemical Society, Washington D.C, pp. 115–163.

Kovscek, A.R., Patzek, T.W., Radke, C.J., 1995. A mechanistic population balance model for transient and steady-state foam flow in Boise Sandstone. Chem. Eng. Sci. 50 (23), 3783–3799.

Lake, L.W., Johns, R.T., Pope, G.A., Rossen, W.R., 2014. Fundamentals of Enhanced Oil Recovery. Society of Petroleum Engineers, Richardson, TX, 2014.

Li, K., 2004. Generalized capillary pressure and relative permeability model inferred from fractal characterization of porous Media. In: Paper SPE 89874 Presented at SPE Annual Technical Conference and Exhibition, Houston, TX, 26–29 September.

Ma, K., Farajzadeh, R., Lopez-Salinas, J.L., Miller, C.A., Biswal, S.L., Hirasaki, G.L., 2014. Non-uniqueness, numerical artifacts, and parameter sensitivity in simulating steady-state and transient foam flow through porous Media. Transp. Porous Media 102 (3), 325–348.

Ma, K., Lopez-Salinas, J.L., Puerto, M.C., Miller, C.A., Biswal, S.L., Hirasaki, G.J., 2013. Estimation of parameters for the simulation of foam flow through porous Media. Part 1: the dry-out effect. Energy & fuels 27 (5), 2363–2375.

Ma, K., Ren, G., Mateen, K., Morel, D., Cordelier, P., 2015. Modeling techniques for foam flow in porous Media. SPEJ 20 (03), 453–470.

Moradi-Araghi, A., Johnston, E.L., Zornes, D.R., Harpole, K.J., 1997. Laboratory evaluation of surfactants for CO2-foam applications at South Cowden unit. In: Paper SPE 37218 Presented at the SPE International Symposium on Oilfield Chemistry, Houston, TX, 18–21 February.

Myers, T.J., Radke, C.J., 2000. Transient foam displacement in the presence of residual oil: Experiment and simulation using a population-balance model.

Industrial Eng. Chem. Res. 39 (8), 2725–2741.
Naderi Beni, A., Varavei, A., Delshad, M., Farajzadeh, E., 2013. Modeling Gas solubility in water for foam propagation in porous Media. In: Paper SPE 163579 Presented at the SPE Reservoir Symposium, Woodland, TX. 10–20 February.
Nguyen, Q.P., Currie, P.K., Buijse, M., Zitha, P.L.J., 2007. Mapping of foam mobility in porous Media. J. Petroleum Sci. Eng. 58 (1–2), 119–132.
Nguyen, Q.P., Rossen, W.R., Zitha, P.L.J., Currie, P.K., 2009. Determination of Gas trapping with foam using X-Ray computed tomography and effluent analysis. SPEJ 14 (02), 222–236. SPE-94764-PA.
Osterloh, W.T., Jante, M.J., 1992. Effects of Gas and liquid velocity on steady-state foam flow at high temperature. In: Paper SPE 24179, Presented at the 1992 SPE/DOE EOR Symposium, Tulsa, OK, April 22–24.
Patzek, T.W., 1988. Description of foam flow in porous Media by the population balance approach. In: Smith, D. (Ed.), Surfactant-based Mobility Control: Progress in Miscible-flood Enhanced Oil Recovery. American Chemical Society, Washington, DC, pp. 326–341 (chapter 16).
Persoff, P., Radke, C.J., Pruess, K., Benson, S.M., Witherspoon, P.A., 1991. A laboratory investigation of foam flow in Sandstone at elevated pressure. SPE Reserv. Eng. 6 (03), 365–372. SPE-18781-PA.
Rossen, W.R., 1996. Foams in enhanced oil recovery. In: Prud'homme, R.K., Khan, S. (Eds.), Foams: Theory, Measurements and Applications. Marcel Dekker, New York.
Rossen, W.R., Gauglitz, P.A., 1990. Percolation theory of creation and mobilization of foam in porous Media. A.I.Ch.E. J. 36 (8), 1176–1188.
Rossen, W.R., Zeilinger, S.C., Shi, J.X., Lim, M.T., 1999. Simplified mechanistic simulation of foam processes in porous Media. SPEJ 4 (03), 279–287. SPE-57678-PA.
Sanchez, J.M., Schechter, R.S., Monsalve, A., 1989. Surfactant effects on the two-phase flow of steam-water and nitrogen-water through permeable Media. J. Petroleum Sci. Eng. 3, 1–2, 185-199.
Schramm, L.L., 1994. Foams: Fundamentals and Applications in the Petroleum Industry, vol. 242. American Chemical Society, Washington, DC.
Shan, D., Rossen, W.R., 2004. Optimal injection strategies for foam IOR. SPEJ 9 (02), 132–150.
Skoreyko, F.A., Villavicencio, A.P., Prada, H.R., Nguyen, Q.P., 2012. Understanding foam flow with a new foam EOR model developed from laboratory and field data of the naturally fractured cantarell field. In: Paper SPE153942 Presented at the 18th SPE Improved Oil Recovery Symposium, Tulsa, OK, 14–18 April.
Vassenden, F., Holt, T., 1998. Experimental foundation for relative permeability modeling of foam. In: Paper SPE 39660 Presented at the SPE/DOE Improved Oil Recovery Symposium, Tulsa, OK. 19–22 April.
Xu, Q., Rossen, W.R., 2003. Effective viscosity of foam in periodically constricted tubes. Colloids Surfaces A Physicochem Eng. Asp. 216, 1–3, 175-194.
Zhou, Z.H., Rossen, W.R., 1995. Applying fractional-flow theory to foam processes at the 'limiting capillary pressure'. SPE Adv. Technol. 3 (01), 154–162. SPE-24180-PA.
Zitha, P.L.J., 2006. A new stochastic bubble population model for foam in porous Media. In: Paper SPE 98976 Presented at the SPE/DOE Symposium on Improved Oil Recover, Tulsa, OK, 22–26 April.